POLITECNICO DI TORINO
Repository ISTITUZIONALE

Modelling electronic transport in monocrystalline metal oxide gas sensors: from the surface kinetics to the experimental response

(Article begins on next page)

10 April 2024

Modelling electronic transport in monocrystalline metal oxide gas sensors: from the surface kinetics to the experimental response

Roberto Guarino [a,1,*], Fabrizio Mo [b,1,*], Yuri Ardesi [b], Andrea Gaiardo [c,*],

Matteo Tonezzer [d,e,*], Sergio Guarino [f], Gianluca Piccinini [b]

[a] École Polytechnique Fédérale de Lausanne (EPFL), Swiss Plasma Center (SPC), CH-5232 Villigen PSI, Switzerland

[b] Department of Electronics and Telecommunications, Politecnico di Torino, Corso Duca degli Abruzzi 24, 10129 Torino, Italy

[c] MNF-Micro Nano Facility Sensors and Devices Centre, Bruno Kessler Foundation, Via Sommarive 18, Trento 38123, Italy

[d] IMEM-CNR, sede di Trento - FBK, Via alla Cascata 56/C, 38123 Trento, Italy

[e] Centre Agriculture Food Environment, University of Trento/Fondazione Edmund Mach, Via Mach 1, 38010 San Michele all'Adige, Italy

[f] Koral Technologies Srl, Via Sanseverino 95, 38122 Trento, Italy

[1] These Authors contributed equally to this work

* Corresponding Authors

(roberto.guarino@epfl.ch, fabrizio.mo@polito.it, gaiardo@fbk.eu, matteo.tonezzer@cnr.it)

Sensor and Actuators B accepted manuscript

Abstract

Gas sensing systems and devices based on metal oxides are widely spreading due to their high performance in terms of sensor response and relatively low costs. Despite several experimental studies, as well as molecular simulations, are available in the literature, a tool that can quickly predict the macroscopic sensor response, and potentially be used for predictive purposes, is still missing.

In this work, we present a modelling approach based on finite-element simulations, using material electrical properties available in the literature. In a first approach, we derive the surface electron trap concentration from fitting the global sensor response. Then, we improve the model by eliminating this fitting and considering the actual time-dependent experimental response. We consider sensors based on single SnO_2 nanowires and show how our model predicts with a good agreement the experimental response *vs.* NO_2, as a function of the working temperature and gas concentration, and also provides many other physical quantities of interest, such as the conduction band edge bending, the space charge and the width of the depletion layer. We further discuss ideas for improving the model and thus increasing its predictive potential.

1 Introduction

Gas-sensing systems are widely employed in a variety of industrial, environmental and biomedical applications. The majority of gas sensors available on the market relies on Metal OXides (MOX), whose response characteristics are based on the variation of the electrical conductivity as function of the gas concentrations and are known since the 1960s [1].

In recent years, thanks to the advances in micro- and nanofabrication technologies, nanostructured metal oxide-based gas sensors have been developed [2,3]. Thanks to an increased surface-to-volume ratio, in fact, they present an enhanced response to various gaseous environments [4-7]. Single nanowire-based devices look extremely promising from this point of view, since the absence of grain boundaries allows for a higher base current which provides improved performance [8,9] and selectivity [10].

Nitrogen dioxide (NO_2) is a toxic and pollutant gas that still exceeds, in many areas across the world, the limits allowed by national and supranational laws [11]. Automotive and industrial emissions are the main NO_2 outdoor sources. It is an air pollutant since it can be associated with severe diseases, such as asthma, lung cancer, and cardiovascular problems [12]. The 15 min - Short Term Exposure Level (STEL) recommended by the Scientific Committee of the European Commission on Occupational Exposure Limits (SCOEL) for NO_2 is 1 ppm. Recently, several works were focused on the development of new sensing materials for the detection of NO_2, owing to the dangerousness of this toxic gas [13,14]. Among them, SnO_2 nanowires showed excellent sensing properties, including high sensing response and good selectivity [15].

The modelling and prediction of the response of semiconductor gas sensors is not trivial and is only partially addressed in the literature. As displayed in Fig. 1, the interaction of a gas with a sensing structure/device is a highly multiscale phenomenon, i.e. it involves different length and time scales, spanning from chemical sub-molecular interactions to the physical manufacturing of the semiconductor and the experimental data acquisition. Several research works are focused on *ab initio* approaches (see, e.g., Refs. [16,17]) or, sometimes, on molecular dynamics (MD) simulations (see, e.g., Refs. [18,19]). Due to their complexity and usually excessive computational cost, these methods can hardly be used as predictive tools or, from an engineering perspective, for designing (and manufacturing) gas sensors.

Therefore, a modelling "brick" linking the molecular behaviour of the sensing structure(s) to the macroscale (i.e. experimental response) is still missing. However, some authors have tried to develop semi-analytical methods for bridging this gap. Barsan *et al.*, for instance, have developed models for capturing the relationship between the conductivity of metal oxide-based sensing layers and the concentration of chemical species. These models have been specifically proposed for nanostructured materials, where the inter-grain contact resistance is taken into account [20,21]. Other Authors, instead, have provided a numerical solution to the Poisson-Boltzmann's equation, with particular choices for the boundary conditions, and applied it to SnO_2 nanowires [22]. Nevertheless, there is still a lack of a comprehensive model for the response of gas sensors, based on a single MOX nanowire, to a specific target gas. In addition, the complexity of physico-chemical

phenomena involved in the sensing mechanism obstacles the realisation and the experimental validation of analytical models.
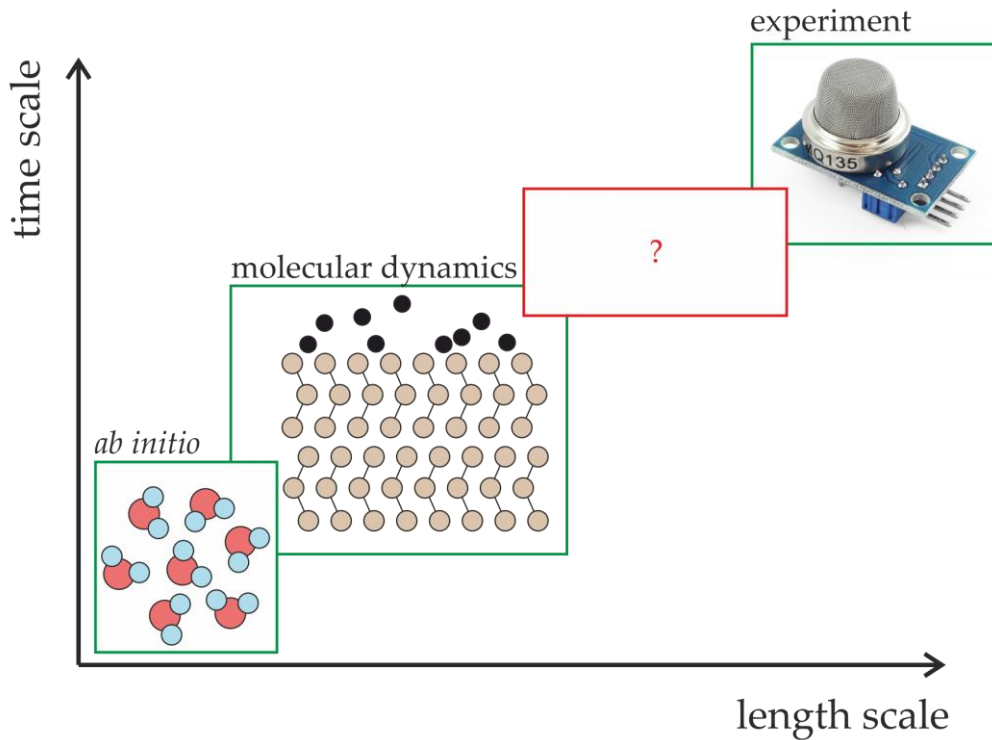

Figure 1: Multiscale approach in gas sensor modelling and missing "brick".

A few recent simulation works have tried to deal with complete MOX gas sensors, but they lack either the prediction of the macroscopic sensor response [23] or the study of the electronic properties [24]. Powroznik *et al.*, instead, have followed a route based on *ab initio* semi-empirical simulations in order to describe the response of $H_2Pc/Pd/PdO$ structures [25].

In order to correctly predict the response of MOX gas sensors, as well as to optimise their performance, it is therefore necessary to develop multiscale models that allow to describe not only the physical/chemical behaviour at the smallest scale, but also to provide a link to the experimental response. In this sense, modelling the electronic transport with "macroscopic" numerical simulations, e.g. based on the finite-element method, can be a powerful tool for considering many physical and technological parameters, as well as for predicting the experimental sensor response linking it to basic physical quantities such as space charge, carrier density, and conduction band bending.

This paper presents a novel modelling approach to MOX gas sensors, specifically tested on SnO_2 single-nanowire sensors, based on finite-element simulations. The main objective of the work is the investigation of the sensing mechanism of MOX sensors, and thus an example system is considered. Specifically, the nanowire geometry has a cylindrical symmetry that simplifies the study and, furthermore, the absence of grain boundaries excludes potential barriers that affect the sensor response, thus only the modulation of the depletion layer takes place.

On one hand, we employ material parameters available in the literature, e.g. extracted from (*ab initio* and/or molecular dynamics) simulations of MOX nanostructures. On the other hand, we extract from the experimental data a few additional macroscopic material parameters, such as the carrier mobility and concentration. In this way, we are able to reproduce the response of SnO_2 nanowires with different diameters, by using one fitting parameter, namely the surface electron trap concentration that emulates the occupied NO_2 adsorption sites. In the second part of the paper, we present an improved model by using an actual experimental time-dependent sensor response to extract such trap concentration. This allows the simulation of SnO_2 sensor response without any fitting parameter. Our model has the advantage of being accurate and close to reality, thanks to the direct solution of the drift-diffusion equations coupled with the Poisson's one. A limitation of the present work is that it is based on the available experimental data, which are collected in a N_2 atmosphere. As future development, which will also test the flexibility of the model, we plan to perform measurements and simulations in the presence of O_2.

2 Experimental and model details

2.1 Background on experimental data and original results

The proposed model was tested by comparing it with the experimental data presented in Ref. [9], whose results are summarised in Fig. 2. The SnO_2 nanowires were grown by chemical vapour deposition in a quartz tube into a horizontal furnace. Pure tin powder and a flow of oxygen were used as sources for the nanowire growth, following the vapour-liquid-solid (VLS) mechanism. A thin layer of Au on SiO_2/Si substrates was used as a catalyst for the growth of the nanowires. The growth temperature controlled the size of the gold droplets and thus the diameter of the nanowires. Morphological and structural characterizations by means of X-Ray Diffraction (XRD), Scanning

Electron Microscopy (SEM) and High-Resolution Transmission Electron Microscopy (HRTEM) demonstrated that SnO_2 nanowires were monocrystalline, without amorphous layers or impurities, and exhibited a large length-to-diameter ratio, as well as a constant diameter. Some nanowires from the same growth process were isolated and contacted at their ends with Ti/Au electrodes, to form chemiresistive sensors. Five sensors based on individual SnO_2 nanowires with different diameters (from 40 to 120 nm, approximately) were tested at different working temperatures towards different concentrations of NO_2 (Fig. 2a). The comparison between the performance of the various sensors, whose only difference was the diameter of the nanowire, made it possible to experimentally test for the first time the detection mechanism called "depletion layer modulation model". The experimental results clearly showed that the sensor response increased as the diameter of the nanowire composing it decreased (Fig. 2b). The response and recovery times, on the other hand, decreased with the working temperature, but it seems that they were not influenced by the diameter of the nanowires (Fig. 2c).

In that work a simple approximation of the bending of the energy bands with a stepwise function was used, considering the outer annular region of the nanowire as completely depleted of electrons, and the inner cylindrical region as unaffected by gas adsorption. The experimental responses of the different sensors were fitted for all the measured gas concentrations, obtaining seven different estimates of the depletion depth (Fig. 2d). All the estimates obtained were in good agreement with a depletion depth of about 13 nm, compatible with the theoretical values in the literature [26,27]. Despite it, these values were obtained by using a very rough approximation. The aim of this work, therefore, is to develop an affordable and reproducible model able to overcome the approximation above-mentioned, and that can be used to predict the sensing performance of MOX gas sensors. Despite the available experimental data cover on a wide range of gas concentrations, the investigation of the sensing mechanism is independent from the gas concentration itself. Additionally, due to the lack of characterizations in Ref. [9] regarding possible defects in the SnO_2 structures, for the development of the model we considered stoichiometric SnO_2 nanowires, therefore without the presence of oxygen or cation vacancies.
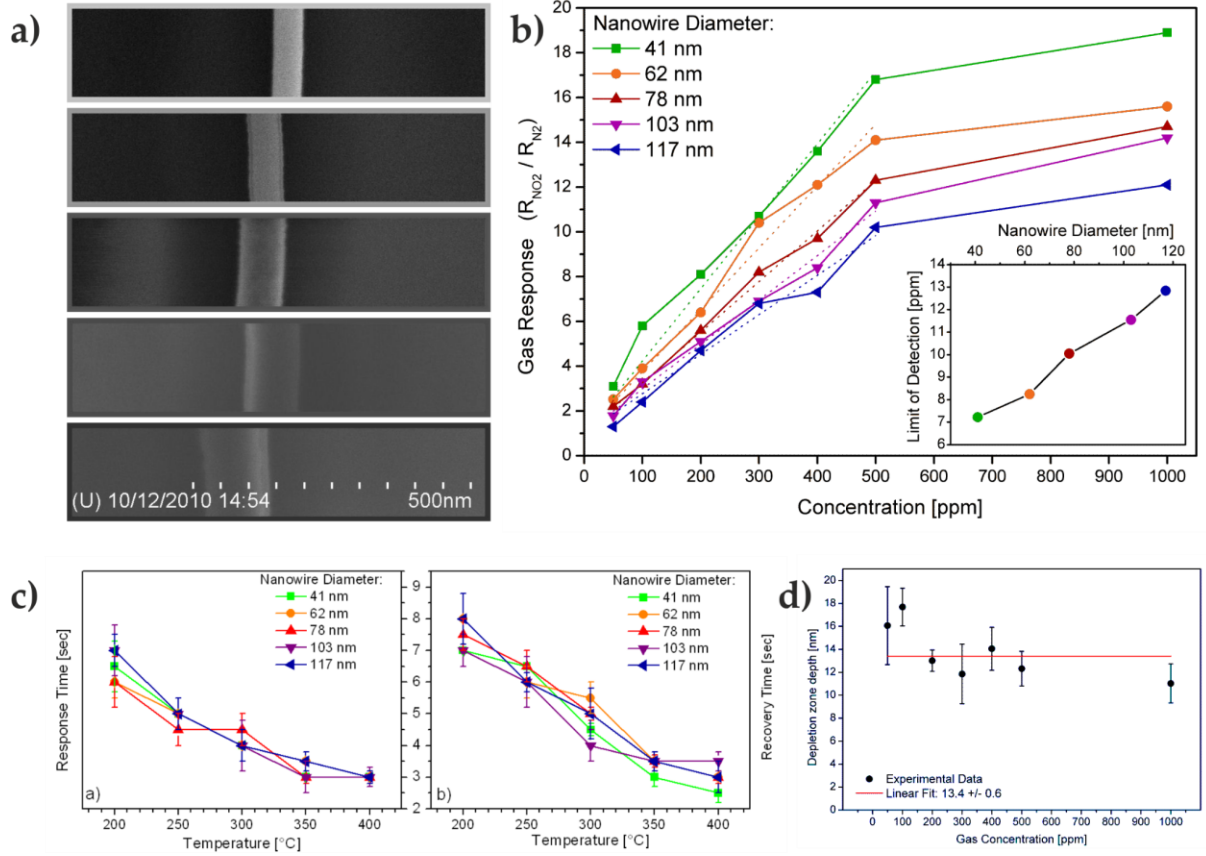
Figure 2: Main results of the original experimental article (Ref. [9]). **a)** SEM images of different nanowires investigated (from bottom to top: 117, 103, 78, 62, and 41 nm). **b)** Gas responses of the five single-nanowire sensors to NO_2 concentrations ranging from 50 ppm to 1000 ppm at 250 °C (limit of detections are reported in the inset). **c)** Response and recovery time of the single-nanowire sensors to NO_2, as a function of the working temperature. **d)** Depletion zone depth, calculated from the fits of the single-nanowire sensors response *vs.* NO_2 concentrations, taking into consideration the nanowire diameters: the weighted average value obtained was 13.4 nm. Reproduced with permission from Ref. [9].

2.2 Introduction to modelling approaches

We present two modelling approaches described in Section 2.3 and 2.4, respectively. In both cases, we use Sentaurus TCAD (Synopsys Inc., Mountain View - CA, United States of America) to solve the Poisson's and the drift-diffusion equations, and we characterise a new material, namely the monocrystalline SnO_2, with specific parameters taken both from literature and experimental evidence, as conceptually depicted in Fig. 3a. We model the surface kinetics and NO_2 molecules adsorption through electron traps placed onto the nanowire surface. In particular, in the first approach (see Section 2.3), we obtain the electron trap density N_T by fitting the sensor

7

experimental responses. This is useful to demonstrate that modelling the sensing phenomenon with an electron trap density is enough to accurately predict the sensor response, bearing in mind the adsorption mechanism of oxidising gases on the surface of thermo-activated MOX sensors [20]. Then (see Section 2.4), we introduce an analytical link between the electron trap density and the sensor dynamic response, i.e. we derive the electron trap density N_T from time-dependent experimental results. The dashed box in Fig. 3a highlights the use of a MATLAB (The MathWorks Inc., Natick - MA, United States of America) script to calculate N_T in the improved model (see Supplementary Information). Fig. 3b schematises the structure of the nanowire and reports its longitudinal 2D section, which is analysed in Sentaurus TCAD. The longitudinal section top face corresponds to the external surface (please note the depleted layer), whereas the bottom face is the nanowire centre axis (rotation axis). Then, we cover the nanowire with an ideal insulator, with relative dielectric permittivity equal to 1.0, in order to create a fictitious material interface. This allows to place interface electron traps onto the nanowire surface in Sentaurus TCAD. The final simulated nanowire structure is displayed in Fig. 3c, which depicts the 2D nanowire simulation domain, covered by the fictitious ideal insulator layer. We repeat the procedure to build nanowires with all the diameters specified in [9], namely 41, 62, 78, 103 and 117 nm. Furthermore, we account for the third dimension through cylindrical boundary conditions applied along the z axis. The simulation of 2D meshes is much more computationally efficient than that of 3D structures. With this procedure we obtain simulation times from a few seconds to a few minutes on a 4-core machine. We also verified that we obtain identical results with the 2D mesh described above and with 3D nanowire structures of the type of Fig. 3b. Finally, the nanowire response is defined as a resistance ratio, which is length-independent, thus no restraint is required for the nanowire length, which is assumed to be 500 nm in all cases.
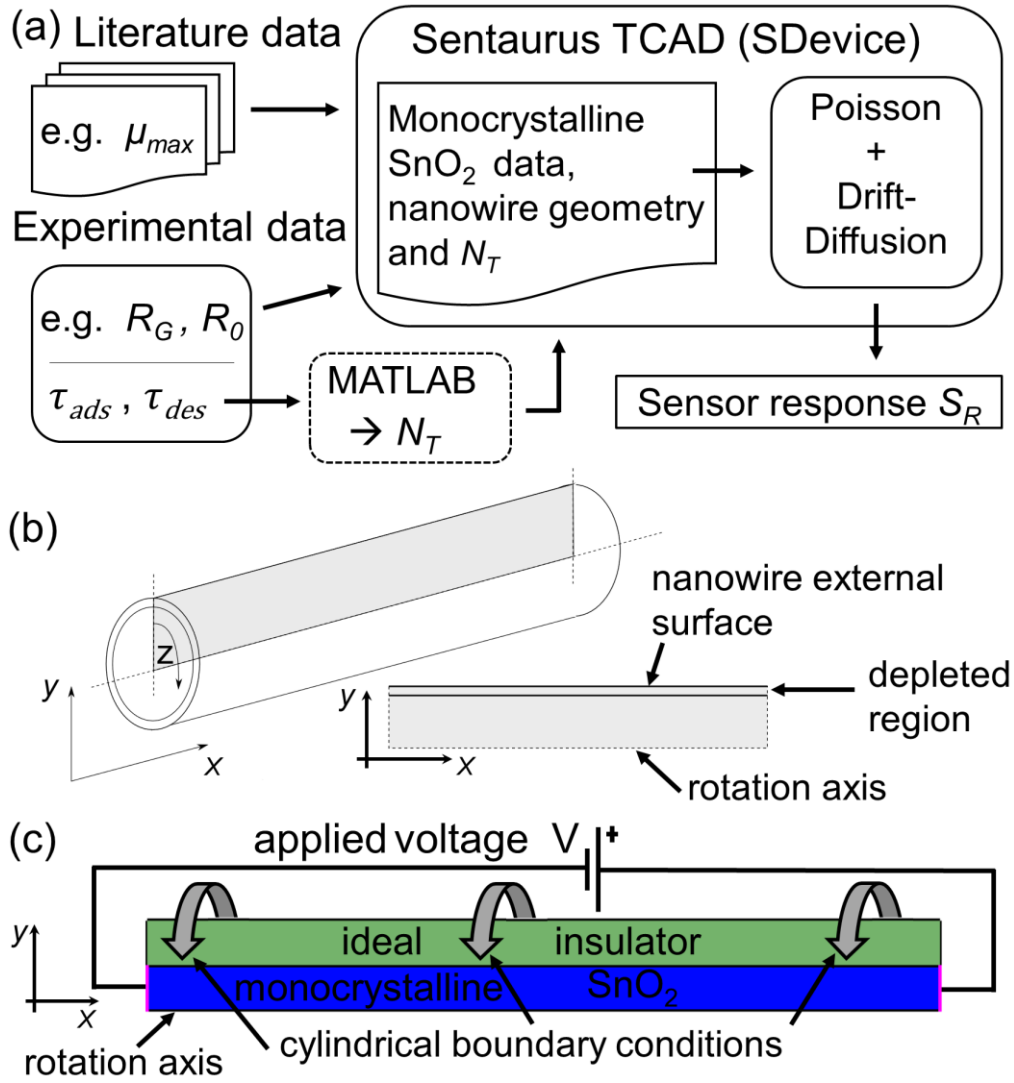
Figure 3: (a) Methodological approach: the dashed box (MATLAB) refers to the improved model of section 2.4; it is used to extract the number of occupied adsorption sites N_T that corresponds to the number of traps in the simulation framework. **(b)** Schematic three-dimensional and cross section view of the considered nanowire structure. **(c)** Sentaurus TCAD model associated with the considered nanowire structure.

2.3 Numerical model with one fitting parameter

In order to accurately model the SnO₂ nanowire response to different NO₂ concentrations at different temperatures, we determine the nanowire electrostatics and transport properties by numerically solving the drift-diffusion equations coupled with the Poisson's one by means of finite element method in Sentaurus TCAD. The considered SnO₂ nanowires behave as classical n-type doped semiconductor resistors. Indeed, quantum confinement effects such as conductance quantization are

not present for the considered diameters and operating conditions, as experimentally verified in [9].

Moreover, we exploited an ideal insulator covering the nanowire with the only purpose of enabling the placement of interface electron traps used to emulate the presence of adsorbed NO_2 molecules onto the SnO_2 nanowire surface. The trap concentration per surface unit N_T (i.e. the density of occupied adsorption sites) changes with the NO_2 concentration and with the temperature, leading to the peculiar temperature-dependent and concentration-dependent sensor response. The adsorbed NO_2 molecules (i.e. the electron traps in the model) oxidise the SnO_2 nanowire surface and generate a space charge, that in turn is responsible for the free carrier concentration modulation that leads to the nanowire conductance modulation [28,29]. This mechanism is accounted for in our model by the aforementioned solution of the drift-diffusion and Poisson's equations.

We extract the most important SnO_2 parameters mainly from the literature [30,31] by referring to the specific crystal orientation specified in [9], *i.e.* a nanowire growth direction parallel to [1 0 0] (see Table S1 in the Supplementary Information). Since the sensor response to oxidising gases is usually defined as $S_R = R_G / R_0$, where R_G is the nanowire resistance under exposure to NO_2 and R_0 is the nanowire resistance in inert environment, the SnO_2 parameters influencing the nanowire resistance value are of crucial importance.

In the majority carrier approximation, the resistance of the nanowire can be written as:

$$R = \frac{1}{q\,n\,\mu}\frac{L}{A} \qquad\qquad (1)$$

where q is the elementary charge, n is the number of free electrons in conduction band, μ the electron mobility, L the nanowire length and A the nanowire cross-section area. Therefore, particular effort should be made in modelling n and μ. The operating conditions, and the fabrication process as well, strongly impact on the concentration of SnO_2 lattice defects, possibly varying n and μ by order of magnitudes [32,33]. In addition, the resistance modulation introduced by NO_2 adsorption is mainly related to a variation of free electron density n due to the created surface space charge and consequent band bending.

We assume that, at room temperature ($T_0 = 300$ K), the longitudinal mobility is $\mu_{max} = 166$ cm^{2}V^{-1}s^{-1}, as calculated by means of *ab initio* techniques for monocrystalline SnO_2 [30]. We approximate the mobility temperature dependence with the one of silicon,

i.e., $\mu(T) = \mu_{max} (T/T_0)^{-2.5}$, due to the lack of specific information in the literature. Additionally, we calculate n to get the same R_0 of the experimental data. In general, it is possible to measure μ and extract n with a similar procedure.

Finally, as mentioned in section 2.2, we emulate the presence of NO_2 by means of interface electron traps that create a space charge in the nanowire and thus modulate the sensor resistance. In Sentaurus, the electron traps are characterised through their energy level and scattering cross-section, from which the electron-trap scattering probability is evaluated and the conduction properties are calculated. We assume the energy difference between the conduction band edge and the trap energy as calculated in [29] by means of *ab initio* techniques. It corresponds to the desorption energy of NO_2 molecules (the desorption process releases electrons back in the conduction band). Then we set the trap-electron interaction cross-section equal to the average NO_2 molecule steric hindrance, estimated as the van der Waals radius of the NO_2 molecule.

In this first model, we fit the number of traps N_T to obtain the experimental sensor response as a function of temperature and NO_2 concentration. In particular, we make use of a dichotomic procedure, starting from an initial guess for N_T, assumed to be equal to the electron concentration n in the nanowire. At each step of the fitting procedure the fully coupled Poisson's and drift-diffusion equations are solved in Sentaurus TCAD with the considered N_T value, and the response of the sensor is calculated and compared with the experimental one. Then N_T is increased/decreased depending if the obtained sensor response results smaller/larger than the experimental one. Initially, N_T is updated by increasing/decreasing it by one order of magnitude, then it is increased/decreased by half of the distance from the last considered value until the calculated response matches the experimental one within a tolerance interval (set to be 0.1 over S_R). The procedure is repeated for each experimental datum, and the obtained N_T values are reported in the Supplementary Information (see Tables S2 and S3).

The purpose is to verify if this computational approach provides reasonable results in terms of accuracy and sensor response prediction capability. Since this is verified (see Section 3), we then eliminate this fitting, as better explained in the next Section.

2.4 Improved numerical model without fitting parameters

The model presented above relies on the fitting of the traps N_T. In this section, we improve the model by eliminating the fitting on N_T. We extract N_T from time-dependent measurements, following the approach reported in [34]. Specifically, according to the first order Langmuir adsorption model [35], and considering the chemistry of NO_2 adsorption reaction, the rate of occupied adsorption sites can be described as:

$$\frac{dN_{occ}(t)}{dt} = k_{ads}[N_{tot} - N_{occ}(t)]C - k_{des}N_{occ}(t) \tag{2}$$

where N_{occ} is the number of occupied adsorption sites, N_{tot} the number of available adsorption sites, C the impinging flux of NO_2 molecules onto the nanowire surface, and k_{ads} and k_{des} are the two rate constants for the NO_2 adsorption and desorption reactions, respectively. Assuming $N_{occ}(0) = 0$, the solution of Equation (2) during the adsorption process reads:

$$N_{occ}(t) = (Ck_{ads} N_{tot})/(Ck_{ads} + k_{des})[1 - exp(-\frac{t}{\tau_{ads}})] = N_{inf}\left(1 - e^{-t/\tau_{ads}}\right) \tag{3}$$

where $N_{inf} = (k_{ads} C N_{tot})/(k_{ads} C + k_{des})$ is the steady state number of occupied adsorption site density, and $\tau_{ads}= 1/(k_{ads} C + k_{des})$ the adsorption time constant. Analogously, during the desorption process, the solution of Equation (2) becomes:

$$\frac{dN_{occ}(t)}{dt} = - k_{des}N_{occ}(t) \quad \Rightarrow \quad N_{occ}(t) = N_{inf}\, e^{-t/\tau_{des}} \tag{4}$$

where $\tau_{des}= 1/k_{des}$ is the recovery process time constant.

In general, a single adsorbed NO_2 molecule may trap one to two electrons, dynamically depending also on the adsorption site occupancy and on the working temperature [31]. In order to keep the model complexity low, we assume that each NO_2 molecule corresponds to a single trap, and thus we fix the trap concentration equal to the steady state occupied adsorption site density, i.e., $N_T = N_{inf}$. It is possible to derive N_{inf} from time transient sensor response measurements as described in the following. The time variation of the electrical resistance $R_G(t)$ in presence of NO_2 follows the adsorption-desorption process time evolution. Indeed, the electrical state of the nanowire is

determined by the amount of depletion within the nanowire itself, and we can expect a typical electrical time response of the order of thermal motion of electrons, *i.e.*, much faster than adsorption and desorption processes (the electron thermal velocity at around 300 K is of the order of 10^5 m s^{-1}). Thus, the depletion width variation rapidly accompanies the variation of surface charge due to the trapping/releasing of an electron by the adsorbed/desorbed NO_2 molecule. A more formal discussion is presented in the Supplementary Information (see Section S1). The main result is that the time evolution of $R_G(t)$ matches well the time evolution of $N_{occ}(t)$. Since the sensor response is defined as $S_R = R_G / R_0$ and since R_0 is constant, $S_R(t)$ follows the same time evolution of $R_G(t)$ and thus of $N_{occ}(t)$. From the experimental time response we extract $R_G(t) = R_0 S_R(t)$ and according to what aforementioned we assume it to be a first-order exponential time evolution, *i.e.*, we assume that it matches the $N_{occ}(t)$ time evolution. Then, we use it to extract the adsorption and the desorption process time constants τ_{ads} and τ_{des} that appear in $N_{occ}(t)$ and thus in $R_G(t)$. We perform the time constant extraction in two different ways: (i) by considering the logarithm of the measured responses and performing a linear interpolation of the experimental curves, similarly to what is done in Ref. [35]; (ii) by estimating the adsorption and desorption time constants by dividing the total transient duration by 5. The latter procedure relies on the well-known observation that first-order time exponential models present only small variations of the order of 0.7% after about 5 times the time constant. The detailed extraction procedures are described in the Supplementary Information (see Section S2 and S3, respectively). The obtained time constants and N_T values are reported in the Supplementary Information (see Tables S4 and S5). From the desorption process time constants, we obtain the desorption rate constants as $k_{des} = 1/\tau_{des}$. Then, from the adsorption process time constants and the desorption rate constant, we obtain the product $C \cdot k_{ads}$, which appears directly in the expression of N_{inf}, as: $C \cdot k_{ads} = (1/\tau_{ads} - k_{des})$. Finally, the steady-state number of occupied adsorption sites is obtained as $N_{inf} = (C\ k_{ads}\ N_{tot})/(C\ k_{ads} + k_{des})$, and it is defined as in Equation (3). As mentioned above, in our model we assume it to be equal to the surface trap concentration N_T. Note that the procedure we adopt to obtain N_T requires the precise extraction (from the experimental data) of the exponential transient time constant τ_{ads} and τ_{des}, which is a challenging task, as we discuss in Section 3.3.

3 Results and discussion

3.1 Sensor current modulation mechanism

The major advantage of simulation-based modelling is that it allows to calculate all the chemical-physical quantities of interest for the analysis of the device (including the space charge, the carrier concentrations, etc.). This enables a deep understanding and performance optimisation of the system investigated.

As a title of example, Fig. 4a reports the electron density in the 41 nm diameter nanowire at 250°C and in presence of 500 ppm of NO_2. The contour diagram in Fig. 4a shows that the nanowire is strongly depleted on its external surface (light blue), with an electron density of the order of 10^{15} cm^{-3}, while it is less depleted in the centre (yellow). This is confirmed in Fig. 4b that reports the electron density in the central cross-section of the nanowire for 500 ppm and for the other considered NO_2 concentrations. The electron density monotonically decreases from the centre ($y = 0$ nm) to the surface ($y = 20.5$ nm) of the nanowire for all the considered NO_2 concentrations. Consequently, a positive charge arises in the nanowire because of the electron depletion, and a space charge is created (see Fig. 3(c)). Since the electron density decreases moving from the nanowire centre toward its surface, the space charge follows the opposite trend by increasing from the nanowire centre toward its surface, according to the depletion level of the nanowire.

This kind of analysis may facilitate the design of the nanowire diameter to optimise the sensor response for a specific application, at a certain temperature and with a certain target concentration, by tuning the extension of the depletion region. Indeed, even though there is a fitting on N_T, the obtained depletion layer and space charge correspond exactly to the depletion region and space charge induced in the nanowire by the presence of adsorbed NO_2 molecules, which allow to reproduce the sensor response in terms of conductance modulation.
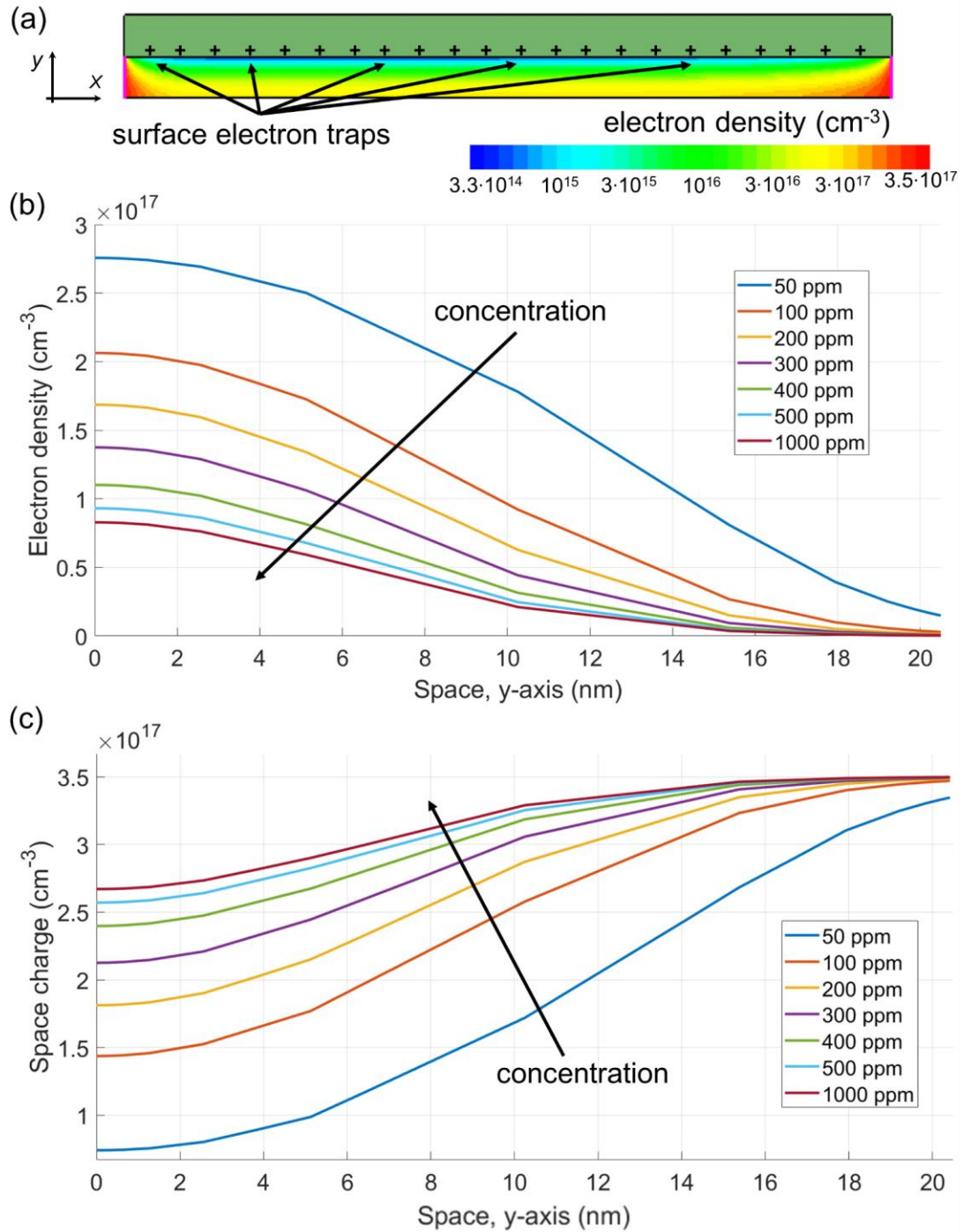
Figure 4: (a) Calculated electron density in the nanowire with diameter 41 nm at 250 °C and 500 ppm of NO_2. The surface electron traps are highlighted for clarity. The picture represents only half of the nanowire and the top line corresponds to the nanowire centre. The green layer is the fictitious insulator covering the nanowire. **(b)** Electron density and **(c)** Space charge density (normalised to $-q$) with different NO_2 concentrations at 250 °C for the 41 nm diameter nanowire in a cut in *x* direction for $x = 250$ nm, plotted in function of the nanowire radius (from $y = 0$ to $y = 20.5$ nm).

Fig.4c displays the calculated normalised space charge in half nanowire at different NO_2 concentrations at 250 °C, for the 41 nm nanowire. By increasing the NO_2 concentration, hence the density of electron traps, the nanowire depletion increases. With the smallest NO_2 concentration (*i.e.*, 50 ppm), the nanowire is only partially depleted and full depletion is not reached even on the surface (instead, full depletion happens for a normalised space charge of $3.5 \cdot 10^{17}$ cm^{-3}, since this equals the free electron density). This justifies the low sensor response that was found experimentally (see Section 3.2) [9].

Increasing the NO_2 concentration to 100 ppm is sufficient to fully deplete the nanowire at the surface, leading to an almost doubled sensor response (see Section 3.2).

Furthermore, if we consider the 500 ppm and 1000 ppm concentrations of NO_2, the nanowire is fully depleted in the range $y \approx 15.5 \div 20.5$ nm. In contrast to the previous two cases (i.e., 50 and 100 ppm), the space charge profiles are very similar, thus forecasting a small n modulation from 500 ppm to 1000 ppm (i.e., small R_G difference and similar sensor response S_R). Fig. 5 verifies our expectations. Specifically, Fig. 5a reports the conduction band edge, whereas Fig. 5b displays the current-voltage characteristics $I(V)$. Since the space charge is linked to the potential profile, and thus to the conduction band bending, through the Poisson's equation, the small space charge variation obtained for 500 and 1000 ppm reflects in a small conduction band bending difference, that is indeed very similar in the two cases (see Fig. 5a). This corresponds to a small n modulation and a small R_G difference, as evident in the similar slopes of the two $I(V)$ curves shown in Fig. 5b.

These results justify the low increase in experimental response found by increasing the NO_2 concentration above 500 ppm, which is explained through a small space charge variation caused by the saturation of the adsorption site occupancy above 500 ppm of NO_2, reducing the nanowire capability to significantly increase the resistance R_G and therefore the response S_R.

The obtained results could guide the technological design of sensors requiring high sensitivity in a high-NO_2 concentration scenario. If the sensor is fabricated in such a way that it has a low n (e.g., through specific stoichiometric ratios or crystalline defects control [33,36]), it is possible to have large space charge, strong conduction band bending and intense n modulation even with few more adsorbed NO_2 molecules, leading to a good sensor sensitivity even at high NO_2 concentrations. The proposed

solution represents a simpler route than other approaches that involve more complex technological challenges, such as decreasing the diameter of the nanowire to increase the surface-to-volume ratio and response, which is usually very tricky due to the poor controllability of the nanowire growth. Therefore, the proposed simulation framework simplifies the evaluation of detection technology alternatives.
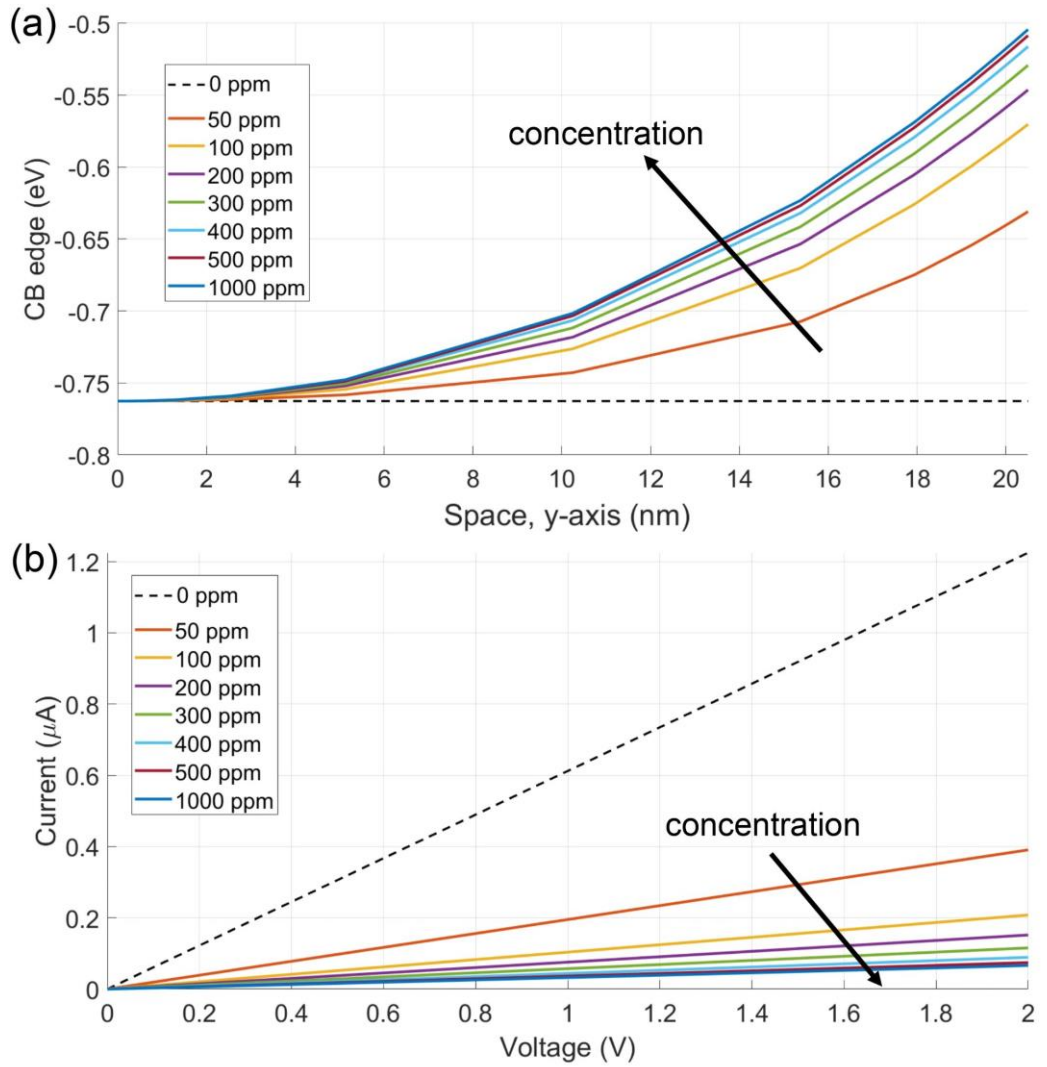
Figure 5: (a) Calculated conduction band edge for different NO_2 concentrations at 250 °C for the 41 nm-diameter nanowire in a cut in x direction (for $x = 250$ nm), as function of the nanowire radius (from $y = 0$ to $y = 20.5$ nm). The conduction band edges are shifted to the equilibrium value (dashed curve) to ease the comparison. **(b)** Current-voltage characteristics at 250 °C for different NO_2 concentrations for the 41 nm-diameter nanowire.

3.2 Numerical modelling with one fitting parameter

Fig. 6 reports the experimental sensor responses S_R and the ones simulated through the first proposed model (see Section 2.3) as a function of temperature and for different nanowire diameters D. The simulated responses are obtained by fitting over N_T to match the experimental data at each temperature for the five nanowires.
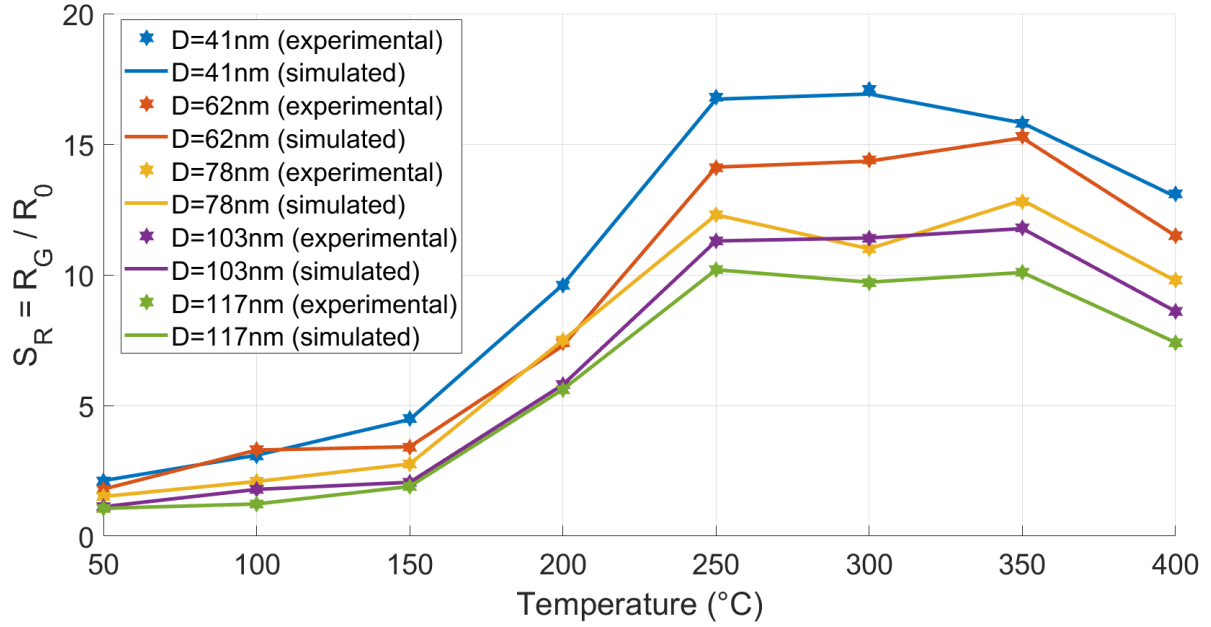

Figure 6 Experimental and simulated sensor responses as function of temperature and for different nanowire diameters, for a constant NO_2 concentration of 500 ppm.

Fig. 7, instead, displays the calculated sensor responses as a function of NO_2 concentration and the relative experimental data at a fixed temperature of 250°C.
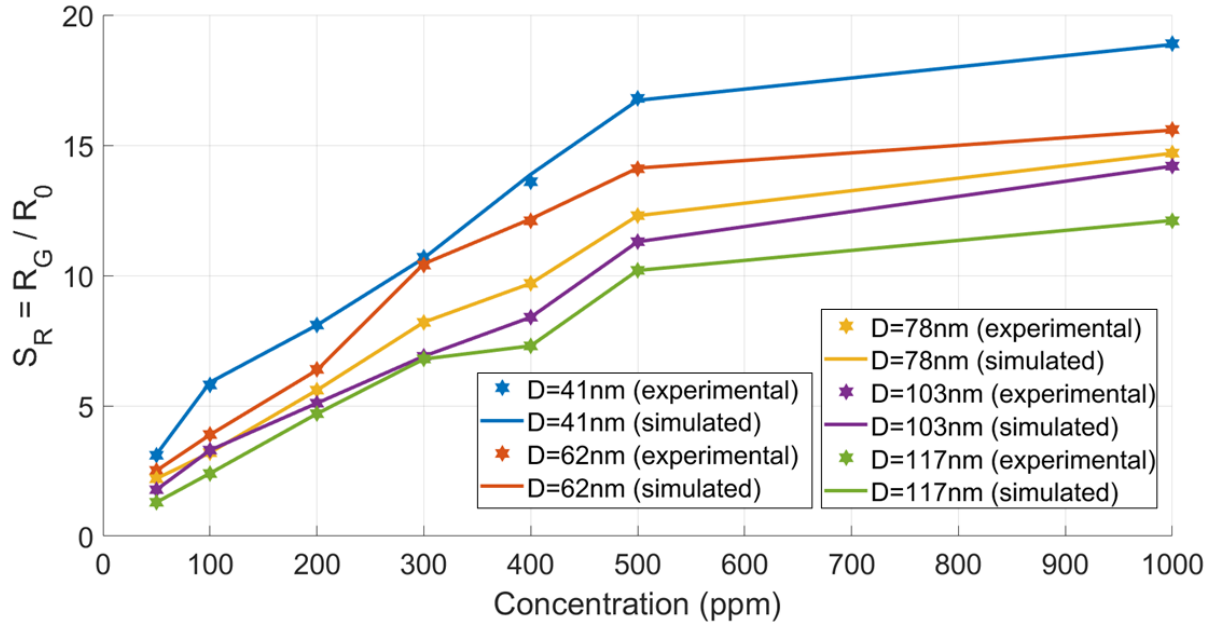
Figure 7: Experimental and simulated sensor responses as function of temperature and for different nanowire diameters, at a temperature of 250 °C.

After the N_T fitting at each temperature and NO_2 concentration, the developed simulation framework is capable of accurately reproducing the sensor response both as a function of the temperature and of the NO_2 concentration, for all the nanowire diameters considered. This means that the usage of interface traps in Sentaurus TCAD is sufficient to accurately reproduce the nanowire surface space charge and the band bending caused by the adsorbed NO_2 molecules. Furthermore, the simulation framework based on the Poisson's and drift-diffusion equations is sufficient to account for the significant physical processes involved. Indeed, the calculated conduction band edge bending, space charge and depletion layer width, accurately correspond to the experimental ones, induced by the adsorption of the NO_2 molecules. Finally, despite the assumption of a silicon-like mobility temperature dependence, the fitting over N_T proves the employed methodology to be an effective way to provide useful information for design purposes, motivating further work to link the N_T with the device physics, eventually removing the need for fitting over N_T.

3.3 Improved model without fitting parameters

In order to eliminate the fitting over N_T, time transient measurements of both the sensing (adsorption) process and the recovery (desorption) process were used. Indeed, as explained in Section 2.4, N_T can be derived from τ_{ads} and τ_{des}. The time-

dependent experimental data available in [9] are relative only to the nanowire with diameter D = 78 nm measured at 500 ppm of NO_2. Furthermore, only a limited temperature range is reported, i.e. between 200°C and 400°C. Fig. 8a and 8b report the calculated sensor responses using the improved model (see Section 2.4). Despite the limited amount of available experimental data, the trend of the computational results obtained with the improved model are in good agreement with the experimental data.
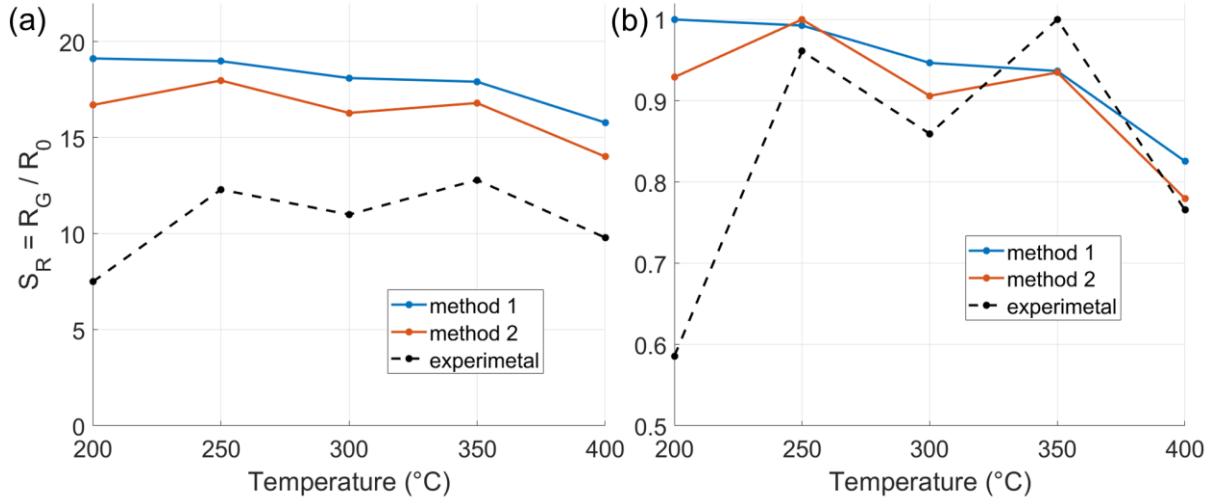
Figure 8: (a) Experimental and simulated sensor response, following two methods for the estimation of the time constants, as function of the temperature, for D = 78 nm and a constant NO_2 concentration of 500 ppm. **(b)** Experimental and simulated sensor responses (normalised), following two methods for the estimation of the time constants, as a function of temperature, for D = 78 nm and a constant NO_2 concentration of 500 ppm.

The procedure we adopt to obtain N_T requires the precise extraction from experimental data of exponential transient time constant. As described in Section 2.4, we evaluate the time constants τ_{ads} and τ_{des} following two different methods, namely a linear interpolation of the (logarithmic) experimental curves and an estimation from the transient duration. Both methods lead to comparable results in terms of accuracy, compared to the experimental data, and predicted response. However, the second method shows a slightly better matching with experimental data.

Even though the time constants obtained with the two methods are similar (see Table S4), there are significant differences on N_T and thus on the final response. In both cases, the simulated responses are about 1.5 times the experimental ones (see Fig. 8a). Furthermore, by observing the results in Fig. 8b, the simulated responses suffer

also of a compressed variation range compared to the experimental one. We attribute the origin of the discrepancy between the calculated and the experimental responses to the following facts:

(a) in our model we assume ideal monocrystalline SnO_2, whereas in reality, nanostructures have many defects which can vary N_{tot} and thus N_T and the final response;

(b) the assumption that each adsorbed NO_2 molecule traps only one electron can influence N_T, that might significantly differ from N_{inf};

(c) the experimental response and recovery times are influenced by the volume and shape of the measurement chamber, and the error on the estimation of the response and recovery time constants influences N_T;

(d) the lack of experimental knowledge about some monocrystalline SnO_2 material parameters for the specific nanowires used, especially on n and μ (and its temperature dependence), impacts on the system electronic electrostatics and transport properties. To improve and further optimise the model, a more precise assessment of N_T is necessary. To this aim, a dedicated work will be carried out, in which experiments will be conducted to obtain a more accurate extraction of τ_{ads} and τ_{des} parameters, as well as further characterisations in order to measure the main material parameters needed as inputs in the simulations, without relying on literature data of analogous nanostructures.

4 Conclusions

In this work, we presented a modelling approach of MOX-based single-nanowire gas sensors based on finite-element simulations, in which we modelled the effects of an oxidising gas through surface electron traps. We initially demonstrated that the simulation framework used is capable of accurately modelling and reproducing the experimental responses of SnO_2 nanowires, with diameters ranging from 41 to 117 nm to different NO_2 concentrations at different temperatures. In order to perform this analysis, we used a fitting over the trap concentration, representing the density of adsorbed NO_2 molecules onto the nanowires.

Then, we improved the model by eliminating the fitting over the trap concentration, instead extracting it from time-dependent experimental results. This improved model provided a good match with the experimental results. We believe that most of the

differences can be overcome through additional and more refined experimental results, which, for instance, could include a larger number of devices, improved electrical contacts, and larger temperature and/or NO_2 concentration ranges.

Therefore, a first objective of future work should be a refinement of the model, in order to estimate more accurately the number of traps. Experiments and *ab initio* calculations, whose results can be easily integrated into the proposed simulation framework, can also be employed for this purpose.

This work demonstrates that the presented methodology is able to capture the main physical-chemical phenomena contributing to the sensing performance of MOX-based sensors. Thus, in principle, it can be extended from single nanowires to also other geometries of monocrystalline sensors, thanks to the model capability of accurately predicting internal quantities such as the conduction band edge bending, the space charge and the width of the depletion layer. This work motivates further research about the direct calculation of the quantities that are currently still derived from experiments, and specific measurement should be performed to determine the temperature dependence of monocrystalline SnO_2 mobility, as well as to estimate more precisely the time constants. The investigation of different material/gas systems is a future objective, as well.

Finally, the model can be used to determine the sensor parameters (e.g. processing/manufacturing conditions and/or geometrical constraints) that influence the sensing performance, thus enabling optimised engineering of future gas sensing devices.

Acknowledgments

References

[1]   T. Seiyama, A. Kato, K. Fujiishi, M. Nagatani, 1962. A new detector for gaseous components using semiconductive thin films. *Analytical Chemistry* **34** 1502-1503.

[2]   A. Bagolini, A. Gaiardo, M. Crivellari, E. Demenev, R. Bartali, A. Picciotto, M. Valt, F. Ficorella, V. Guidi, P. Bellutti, 2019. Development of MEMS MOS gas

sensors with CMOS compatible PECVD inter-metal passivation. *Sensors and Actuators B: Chemical* **292** 225-232.

[3]   A. Gaiardo, D. Novel, E. Scattolo, M. Crivellari, A. Picciotto, F. Ficorella, E. Iacob, A. Bucciarelli, L. Petti, P. Lugli, A. Bagolini, 2021. Optimization of a low-power chemoresistive gas sensor: Predictive thermal modelling and mechanical failure analysis. *Sensors* **21** 783.

[4]   G. Korotcenkov, 2007. Metal oxides for solid-state gas sensors: what determines our choice? *Materials Science and Engineering B* **139** 1-23.

[5]   Z.R. Dai, J.L. Gole, J.D. Stout, Z.L. Wang, 2002. Tin oxide nanowires, nanoribbons, and nanotubes. *Journal of Physical Chemistry B* **106** 1274-1279.

[6]   C.S. Moon, H. Kim, G. Auchterlonie, J. Drennan, J. Lee, 2008. Highly sensitive and fast responding CO sensor using SnO_2 nanosheets. *Sensors and Actuators B: Chemical* **131** 556-564.

[7]   G. Zonta, G. Anania, M. Astolfi, C. Feo, A. Gaiardo, S. Gherardi, A. Giberti, V. Guidi, N. Landini, C. Palmonari, A. de Togni, C. Malagù, 2019. Chemoresistive sensors for colorectal cancer preventive screening through fecal odor: Double-blind approach. *Sensors and Actuators B: Chemical* **301** 127062.

[8]   F. Hernández-Ramírez, A. Tarancón, O. Casals, J. Arbiol, A. Romano-Rodríguez, J.R. Morante, 2007. High response and stability in CO and humidity measures using a single SnO_2 nanowire. *Sensors and Actuators B: Chemical* **121** 3-17.

[9]   M. Tonezzer, N.V. Hieu, 2012. Size-dependent response of single-nanowire gas sensors. *Sensors and Actuators B: Chemical* **163** 146-152.

[10]   M. Tonezzer, 2019. Selective gas sensor based on single SnO_2 nanowire. *Sensors and Actuators B: Chemical* **288** 53-59.

[11]   C. Guerreiro, A.G. Ortiz, F. de Leeuw, M. Viana, J. Horálek, 2016. *Air quality in Europe-2016 report.* Publications Office of the European Union.

[12] Y.O. Khaniabadi, G. Gourdazi, S.M. Daryanoosh, A. Borgini, A. Tittarelli, A. De Marco, 2017. Exposure to PM_{10}, NO_2, and O_3 and impacts on human health. *Environmental Science and Pollution Research* **24** 2781-2789.

[13] S. Kumar, V. Pavelyev, P. Mishra, N. Tripathi, P. Sharma, F. Calle, 2020. A review on 2D transition metal di-chalcogenides and metal oxide nanostructures based NO_2 gas sensors. *Materials Science in Semiconductor Processing* **107** 104865

[14] S.W. Lee, W. Lee, Y. Hong, G. Lee, D.S. Yoon, 2018. Recent advances in carbon material-based NO_2 gas sensors. *Sensors and Actuators B: Chemical* **255** 1788-1804.

[15] H.J. Kim, S.B. Jo, J.H. Ahn, B.W. Hwang, H.J. Chae, S.Y. Kim, J.S. Huh, D. Ragupathy, S.C. Lee, J.C. Kim, 2019. SnO_2 nanowire gas sensors for detection of ppb level NO_x gas. *Adsorption* **25** 1259-1269.

[16] S. Peng, K. Cho, P. Qi, H. Dai, 2004. Ab initio study of CNT NO_2 gas sensor. *Chemical Physics Letters* **387** 271-276.

[17] S.P. Oberegger, O.A.H. Jones, M.J.S. Spencer, 2017. Effect of nanostructuring of ZnO for gas sensing of nitrogen dioxide. *Computational Materials Science* **132** 104-115.

[18] M. Kharatha, A. Vaez, A.S.H. Rozatian, 2013. Molecular dynamics simulation of gas adsorption on defected graphene. *Molecular Physics* **111** 3726-3732.

[19] N.E. Boboriko, Y.U. Dzichenka, 2021. Molecular dynamics simulation as a tool for prediction of the properties of TiO_2 and TiO_2:MoO_3 based chemical gas sensors. *Journal of Alloys and Compounds* **855** 157490.

[20] N. Barsan, U. Weimar, 2001. Conduction model for metal oxide gas sensors. *Journal of Electroceramics* **7** 143-167.

[21] N. Barsan, C. Simion, T. Heine, S. Pokhrel, U. Weimar, 2010. Modeling of sensing and transduction for p-type semiconducting metal oxide based gas sensors. *Journal of Electroceramics* **25** 11-19.

[22] M.Z. Asadzadeh, A. Köck, M. Popov, S. Steinhauer, J. Spitaler, L. Romaner, 2019. Response modeling of single SnO_2 nanowire gas sensors. *Sensors and Actuators B: Chemical* **295** 22-29.

[23] P. Andrei, L.L. Fields, J.P. Zheng, Y. Cheng, P. Xiong, 2007. Modeling and simulation of single nanobelt SnO_2 gas sensors with FET structure. *Sensors and Actuators B: Chemical* **128** 226-234.

[24] F. Yaghouti Niyat, M. Shahrokh Abadi, 2018. COMSOL-based modeling and simulation of SnO_2/rGO gas sensor for detection of NO_2. *Scientific Reports* **8** 2149.

[25] P. Powroznik, L. Grządziel, W. Jakubik, M. Krzywiecki, 2018. Sarin-simulant detection by phthalocyanine/palladium structures: From modeling to real sensor response. *Sensors and Actuators B: Chemical* **273** 771-777.

[26] H. Ogawa, M. Nishikawa, A. Abe, 1982. Hall measurement studies and an electrical conduction model of tin oxide ultrafine particle films. *Journal of Applied Physics* **53** 4448-4455.

[27] J.F. McAleer, P.T. Moseley, J.O.W. Norris, D.E. Williams, 1987. Tin dioxide gas sensors. Part 1 - Aspects of the surface chemistry revealed by electrical conductance variations. *Journal of the Chemial Society, Faraday Transactions 1* **83** 1323-1346.

[28] S. Das, V. Jayaraman, 2014. SnO_2: A comprehensive review on structures and gas sensors. *Progress in Materials Science* **66** 112-255.

[29] S. Gomri, J.L. Seguin, J. Guerin, K. Aguir, 2006. Adsorption–desorption noise in gas sensors: Modelling using Langmuir and Wolkenstein models for adsorption. *Sensors and Actuators B: Chemical* **114** 451-459.

[30] Y. Hu, J. Hwang, Y. Lee, P. Conlin, D.G. Schlom, S. Datta, K. Cho, 2019. First principles calculations of intrinsic mobilities in tin-based oxide semiconductors SnO, SnO_2, and Ta_2SnO_6. *Journal of Applied Physics* **126** 185701.

[31] M. Epifani, J.D. Prades, E. Comini, E. Pellicer, M. Avella, P. Siciliano, G. Faglia, A. Cirera, R. Scotti, F. Morazzoni, J.R. Morante, 2008. The role of surface oxygen vacancies in the NO_2 sensing properties of SnO_2 nanocrystals. *The Journal of Physical Chemistry C* **112** 19540-19546.

[32] D.V. Christensen, M. von Soosten, F. Trier, T.S. Jespersen, A. Smith, Y. Chen, N. Pryds, 2017. Controlling the carrier density of $SrTiO_3$-based heterostructures with annealing. *Advanced Electronic Materials* **3** 1700026.

[33] M.W. Ahn, K.S. Park, J.H. Heo, J.G. Park, D.W. Kim, K.J. Choi, J.H. Lee, S.H. Hong, 2008. Gas sensing properties of defect-controlled ZnO-nanowire gas sensor. *Applied Physics Letters* **93** 263103.

[34] N.M. Vuong, D. Kim, H. Kim, 2015. Surface gas sensing kinetics of a WO_3 nanowire sensor: Part 1—oxidizing gases. *Sensors and Actuators B: Chemical* **220** 932-941.

[35] I. Langmuir, 1918. The adsorption of gases on plane surfaces of glass, mica and platinum. *Journal of the American Chemical Society* **40** 1361-1403.

[36] J.B.K. Law, J.T.L. Thong, 2008. Improving the NH_3 gas sensitivity of ZnO nanowire sensors by reducing the carrier concentration. *Nanotechnology* **19** 205502.

Modelling electronic transport in monocrystalline metal oxide gas sensors: from the surface kinetics to the experimental response

Roberto Guarino [a,1,*], Fabrizio Mo [b,1,*], Yuri Ardesi [b], Andrea Gaiardo [c,*],
Matteo Tonezzer [d,e,*], Sergio Guarino [f], Gianluca Piccinini [b]

[a] École Polytechnique Fédérale de Lausanne (EPFL), Swiss Plasma Center (SPC),
CH-5232 Villigen PSI, Switzerland

[b] Department of Electronics and Telecommunications, Politecnico di Torino, Corso
Duca degli Abruzzi 24, 10129 Torino, Italy

[c] MNF-Micro Nano Facility Sensors and Devices Centre, Bruno Kessler Foundation,
Via Sommarive 18, Trento 38123, Italy

[d] IMEM-CNR, sede di Trento - FBK, Via alla Cascata 56/C, 38123 Trento, Italy

[e] Centre Agriculture Food Environment, University of Trento/Fondazione Edmund
Mach, Via Mach 1, 38010 San Michele all'Adige, Italy

[f] Koral Technologies Srl, Via Sanseverino 95, 38122 Trento, Italy

[1] These Authors contributed equally to this work

* Corresponding Authors (roberto.guarino@epfl.ch, fabrizio.mo@polito.it,
gaiardo@fbk.eu, matteo.tonezzer@cnr.it)

Supplementary Information

S1 Time response of the nanowire electrical resistance

S1.1 General case

Since R_0 is constant, the sensor time response follows the electrical resistance time response $R_G(t)$: $S_R(t) = R_G(t) / R_0$.

In the majority carrier approximation: $R_G(t) = L/(q\,\mu\,n_G(t)\,A)$; where q is the elementary charge (constant), L and A are the length and cross-sectional area of the nanowire, respectively, μ is the electron mobility that we assume constant in time (and constant also under depletion condition), and $n_G(t)$ is the electron concentration in the nanowire in presence of the target gas. The mechanism that permits the resistance modulation is the adsorption/desorption of the target gas from the nanowire surface, with consequent surface charge modulation. This, in turns, creates a space charge close to the nanowire surface that has the effect of producing a band bending and thus an $n_G(t)$ modulation and an $R_G(t)$ time variation.

In this Section, we are interested in the time response of the sensor, and in particular in its relation with the adsorption/desorption process time evolution, given by Equations (3) and (4). Therefore, we solve the Poisson's equation in the general case in two steps of integration (*i.e.*, field and potential) and we verify that the dominant contribution to the sensor time response is due to the kinetics of adsorption/desorption processes, being thus τ_{ads} and τ_{des} the dominant time constants in the first-order exponential response model, or single pole approximation.

We assume that the charge exchange occurs only between the nanowire and the adsorbed/desorbed NO_2 molecules. Therefore, during adsorption, each NO_2 captures an electron to create the NO_2^- ion and generates a negative elementary charge on the surface of the nanowire, compensated by a positive elementary charge in the nanowire close to the surface. Furthermore, we assume the adsorbed NO_2 molecules to be uniformly distributed over the whole nanowire surface and length, thus a cross-section is homogeneous to all the others. We denote with $r = D/2$ the nanowire radius. The charge conservation implies that:

$$q\,N_{occ}(t) \;=\; q\,\int_0^r \rho(y,t)\,dy \quad\Leftrightarrow\quad N_{occ}(t) \;=\; \int_0^r \rho(y,t)\,dy \qquad\qquad (s1)$$

The Poisson's equation for the electric field E is:

$$\frac{dE}{dy} = \frac{\rho(y)}{\varepsilon} \tag{s2}$$

where ε is the SnO$_2$ permittivity.

We assume never to reach the full depletion of the nanowire, meaning that the neutrality implies a null electric field in the centre of the nanowire at $y = 0$. With this boundary condition, the Poisson's equation is:

$$E(y) = \frac{q}{\varepsilon} \int_0^y \rho(y')\, dy' \tag{s3}$$

which, for $y = r$, becomes:

$$E(r) = \frac{q}{\varepsilon} \int_0^r \rho(y)\, dy = \frac{q}{\varepsilon} N_{occ}(t) \tag{s4}$$

By integrating the electric field we obtain the electric potential V, with boundary condition $V(0) = 0$ (arbitrarily chosen as integration constant):

$$\frac{dV}{dy} = -E(y) \quad \rightarrow \quad V(y) = -\frac{q}{\varepsilon} \int_0^y \int_0^Y \rho(y')\, dy'\, dY \tag{s5}$$

We are interested in the time response of the electron concentration $n_G(t)$, that depends on the total band bending in the nanowire, from $y = 0$ to $y = r$. Indeed the $n_G(t)$ modulation is provided by:

$$n_G(t) = n_0\, e^{qV_s/kT} \tag{s6}$$

where k is the Boltzmann's constant, T the temperature, n_0 is the equilibrium electron concentration (in an inert environment) and $V_s = V(r)$ is the surface potential. From Equations (s4) and (s5), we obtain:

$$V_s = -\frac{q}{\varepsilon} \int_0^r N_{occ}\, dy = -\frac{q}{\varepsilon}\, r\, N_{occ} \tag{s7}$$

The first integration in *y* eliminates the dependence on it, leading to a geometry-independent N_{occ}, since it depends only on time. Thus, we get a time dependent surface potential $V_s(t) = -\frac{q}{\varepsilon} r N_{occ}(t)$. Therefore:

$$n_G(t) = n_0 e^{qN_{occ}(t)/kT} \quad and \quad R_G(t) = \frac{L}{q \mu A n_0} e^{-qN_{occ}(t)/kT} \qquad (s8)$$

For the adsorption process, N_{occ} is given by:

$$N_{occ}(t) = N_{inf} \left[1 - e^{-t/\tau_{ads}}\right] \qquad (s9)$$

from which:

$$R_G(t) = \frac{L}{q \mu A n_0} e^{-qN_{inf}/kT} e^{qN_{inf}e^{-t/\tau_{ads}}/kT} = const \cdot e^{qN_{inf}e^{-t/\tau_{ads}}/kT} \qquad (s10)$$

This last equation highlights that the electrical resistance time dependence is in general given by a double exponential relation with time *t*. This means that the system responds very fast to adsorption state variations. In other words, the electrical response of the system is much faster than the adsorption process response, thanks to a double exponential dependence instead of an exponential dependence. The system is able to compensate very rapidly for a variation of the adsorption state, meaning that the dominant contribution in the total time response (the slowest one) is the one due to adsorption kinetics. Therefore, the total system time response is well approximated by a single-exponential response, corresponding exactly to the adsorption process time response. To better clarify this crucial point, we consider the Taylor expansion of Equation (s10):

$$R_G(t) \propto \left[1 + \left(\frac{q N_{inf}}{kT}\right) e^{-t/\tau_{ads}} + \frac{1}{2}\left(\frac{q N_{inf}}{kT}\right)^2 e^{-2t/\tau_{ads}} + \frac{1}{6}\left(\frac{q N_{inf}}{kT}\right)^3 e^{-3t/\tau_{ads}} + \dots\right] \qquad (s11)$$

The first term of the expansion highlights that within the single pole approximation the system response is mainly determined by the adsorption time constant, with a first-order exponential time response like $N_{occ}(t)$.

We stress that τ_{ads} is the adsorption process time constant. Nevertheless, within the first-order exponential model for the sensor response, it corresponds also to the sensor sensing process time constant, since the sensor response presents the same time evolution of $R_G(t)$. Also, it should be noted that the sensing process time constant is not the sensor sensing time, even if the two are related. The sensing time is an experimental measure commonly defined as the time taken to achieve 90% of the response. Instead, the time constant of a first order exponential time response, like the considered sensing process, is by definition the time interval at which the sensor response is exactly 1/e times the initial one.

In the case of the desorption process an analogous argument holds, the only difference is in the specific expression of $N_{occ}(t)$ to be considered in Equation (s8), and the fact that τ_{des} characterises the time response of the sensor in the very same fashion as τ_{ads} does for the adsorption case.

Finally, note also that a very similar result can be obtained within the depletion approximation as described in Ref. [35] and as we briefly summarise in the next Section.

S1.2 Depletion approximation

In this Section, we recover a similar result starting from the depletion approximation of the nanowire, we proceed similarly to what is done in Ref. [35]. Specifically, we add the assumption that there is an abrupt transition between the fully depleted region close to the surface of the nanowire and the neutral region in the centre of the nanowire, with a null transition region. The charge neutrality implies that, at each time instant t, the number of occupied adsorption sites N_{occ} over the lateral nanowire surface equals the total space charge in the nanowire, *i.e.*:

$$2\pi r\, L\, q\, N_{occ}(t)\ =\ q\, n_0 \pi\, L\, [r^2 - y_D^2(t)] \qquad\qquad (s12)$$

where n_0 is the equilibrium electron concentration (*i.e.*, it is equal to the number of elementary charges per unit volume present in the depleted region) and y_D indicates the transverse coordinate at which the full depletion condition starts. Under the depletion approximation perspective, the R_G modulation (neglecting the conduction in the depleted region) is governed by a modulation of the conducting cross section A_G

that is varied instead of n in the R_G expression $R_G(t) = L \, / \, (q \, \mu \, n_0 \, A_G(t))$. Considering that $A_G(t) = \pi \, [r^2 - y_D^2(t)]$, it follows:

$$R_G(t) \; = \; \frac{L}{q \, \mu \, n_0 \, \pi \, [r^2 - y_D^2(t)]} \; = \; \frac{L}{q \, \mu \, 2 \, \pi \, r \, N_{occ}(t)} \qquad\qquad (s13)$$

which, in the adsorption case, becomes:

$$R_{G,ads}(t) \; = \; \frac{L}{q \, \mu \, 2 \, \pi \, r \, N_{inf}} \, \left[\frac{1}{1 - e^{-t/\tau_{ads}}} \right] \qquad\qquad (s14)$$

whereas in the desorption case becomes:

$$R_{G,des}(t) \; = \; \frac{L}{q \, \mu \, 2 \, \pi \, r \, N_{inf}} \, \left[e^{t/\tau_{des}} \right] \qquad\qquad (s15)$$

Note that in both cases the electrical resistance time constant is equal to the adsorption/desorption process one with a single exponential dependence on it, *i.e.*, the sensor responds as a first-order exponential system.

S2 Time constant extraction through linear interpolation

In Sections S1.1 and S1.2, we showed that the adsorption/desorption kinetics is converted in a resistance modulation through a mechanism that preserves the time constants, meaning that the sensor time response is approximately the same as the adsorption/desorption kinetics. Under this assumption, the time evolution of R_G and S_R is of the kind of first-order exponential.

Therefore, the measured adsorption/desorption transients can be fitted with an exponential function to extract the time constants. Nevertheless, due to the low number of time samples in the measure dataset, the fitting over the exponential function would be affected by a large numerical error, leading to barely reliable τ_{ads} and τ_{des} values. As described in Ref. [35], a more reliable fitting can be obtained by taking the natural logarithm of the sensor response and by fitting it by a straight line. We implemented this procedure in a MATLAB script, as described in the following. The reference experimental data report $S_R(t)$ from which we extract $R_G(t) = R_0 S_R(t)$. During the adsorption transient, the sensor resistance $R_G(t)$ increases in time from the initial value (in an inert environment) to the steady-state value for the considered NO$_2$

concentration and operating temperature. We denote the steady-state final R_G value with $R_{G,max}$ and we evaluate the ratio $R_G(t)/R_{G,max}$ under the depletion approximation from Equation (s13), *i.e.*:

$$\frac{R_G(t)}{R_{G,max}} = \frac{1}{1-e^{-t/\tau_{ads}}} \qquad (s16)$$

T

o ease the fitting procedure we consider the conductance ratio $\frac{G_{G,max}}{G_G(t)} = 1 - e^{-t/\tau_{ads}}$ and we consider its natural logarithm to have a linear dependence from time t, thus:

$$ln\left(1 - \frac{G_{G,max}}{G_G(t)}\right) = -\frac{t}{\tau_{ads}} \qquad (s17)$$

Equation (s16) is then fitted in MATLAB through a first-order polynomial function, from which we obtain the adsorption time constant τ_{ads}.

For the desorption process, we consider again the ratio $R_G(t)/R_{G,max}$ where this time $R_{G,max}$ is the initial resistance value in steady-state conditions when the target gas NO_2 is present. During the desorption process $R_G(t)$ decreases from $R_{G,max}$ to the final value, corresponding to the value in an inert environment. From Equation (s14) under the depletion approximation, we get:

$$\frac{R_G(t)}{R_{G,max}} = e^{t/\tau_{des}} \qquad (s18)$$

We consider again its natural logarithm to have a linear dependence with time t, thus:

$$ln\left(\frac{R_G(t)}{R_{G,max}}\right) = \frac{t}{\tau_{des}} \qquad (s19)$$

Equation (s18) is then again fitted in MATLAB through a first-order polynomial function, from which we obtain the desorption time constant τ_{des}.

The final values of τ_{ads} and τ_{des} are then calculated as the arithmetic mean over all considered transient time constants, for the considered NO_2 concentration and temperature.

An example of the implemented procedure is reported in Fig. S1. The obtained values of τ_{ads} and τ_{des} are reported in Table S4.
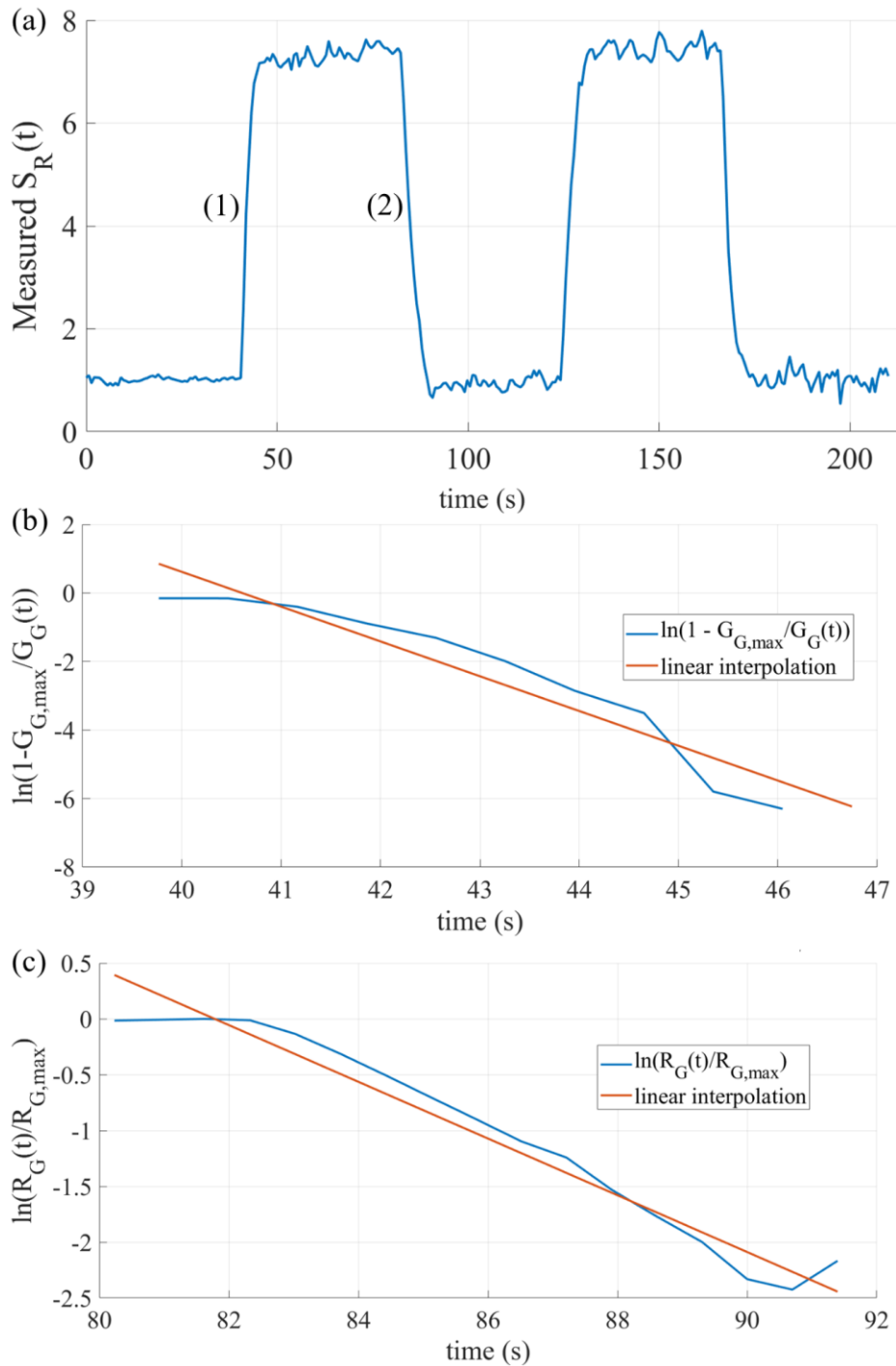

Figure S1: (a) Experimental sensor response $S_R(t)$ for D=78 nm, at a constant concentration of 500 ppm of NO_2 and at a temperature of 200 °C; **(b)** Linear interpolation of the first rising edge indicated with (1) in (a); **(c)** Linear interpolation of the first falling edge indicated with (2) in (a).

S3 Time constant extraction from the transient duration

Another approach we propose to extract the adsorption and desorption time constants from the experimental time measurements relies again on the observation that the first-order term in equation (s10) is a first-order exponential response with time constant τ_{ads} (and τ_{des} for the desorption case). Instead of considering the analytical expression of $R_G(t)$, it is possible to observe that the typical transient response of first order time exponential system models presents only small variations of the order of 0.7% after about 5 times the time constant. Therefore, we implemented a MATLAB script to extract the total transient duration within the tolerance of 0.7% over the maximum overshoot. Specifically, the script considers the time transient and identifies two time instants: the first one is the starting time instant t_i, corresponding to time instant at which the sensor response starts to sharply change its value from the initial constant one; the second one corresponds to the final time instant t_f, corresponding to the time instant at which the sensor response start presenting oscillations smaller than the 0.7% of the total excursion from t_i to t_f. The total transient duration is then calculated as $\Delta t = t_f - t_i$ and the relative time constant is assumed to be $\Delta t/5$. The final values of τ_{ads} and τ_{des} are then calculated as the arithmetic mean over all considered transient time constants for the considered NO_2 concentration and temperature.

An example of the implemented procedure is reported in Fig. S2. The obtained values of τ_{ads} and τ_{des} are reported in Table S4.
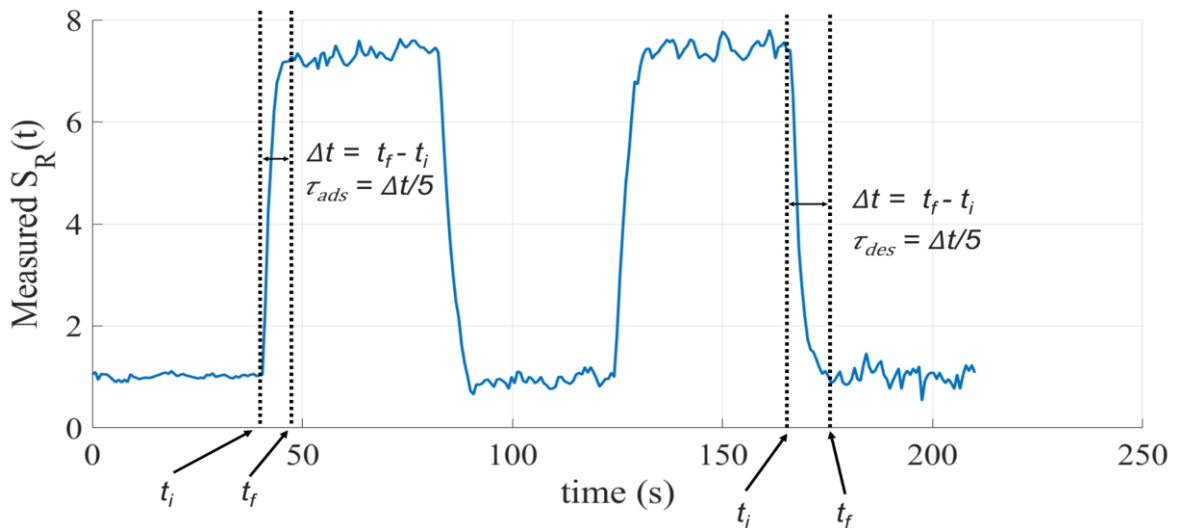

Figure S2: Experimental sensor response $S_R(t)$ for D=78 nm, at a constant concentration of 500 ppm of NO_2 and at a temperature of 200 °C. The vertical dashed lines highlight the initial and final time instants for the first rising edge and for the second falling edge.

S4 Sentaurus TCAD models

In this Section, we report details on the physical models activated in Sentaurus TCAD and the mathematical methods and parameters used to perform the simulation results reported in this work. The used default models/settings are not reported.

PMI models:
         Physics

                  EffectiveIntrinsicDensity(NoBandGapNarrowing)
                  Mobility(ConstantMobility)
Temperature= 300   # K

Physics (Material Interface: SnO$_2$ - Ideal insulator interface)
Traps
EnergyMid=0.775   # eV
eXsection=9.4e-15   # cm^2
 # hXsection is not enabled

Numerical methods:
         Math

                  TrapDLN = 13   * Number of discrete TrapElevels with which it is
                             approximated the energy distribution of electron traps
                  Cylindrical   * Cylindrical coordinates are used
                  Extrapolate   * Last 2 iteration results are used as initial guess for the new
                                 one
                  RelErrControl   * Self-consistent loop updating - numerical error handling
                  Iterations=60   * Maximum number of Newton method iterations per bias step

Algorithms/Strategies (equilibrium and non-equilibrium):
         Solve
                  Poisson
Coupled { Poisson Electron Hole }

Quasistationary

MaxStep=0.05

InitialStep=0.05

MinStep = 0.001

Goal { Name="drain" Voltage=2.0}

S5 Supplementary tables and data

TABLE S1. Mine SnO_2 material electrical parameter values used to perform the simulations. Optical parameters are not reported.

Parameter	Value	Notes
relative permittivity	2.28	isotropic approximation, it is in the range 2.26÷2.30, from [SR1]
lattice heat capacity	2.45 J K^{-1} cm^{-3}	from [SR2]
lattice thermal conductivity	0.765 W m^{-1} K^{-1}	isotropic approximation (average), from [SR3]
band gap	3.74 eV	from [SR4]
electron affinity	5.73 eV	in the range 4.04÷5.73 eV depending on crystal orientation, from [SR5]
electron DOS effective mass	0.26	for longitudinal direction only, from [SR6]
hole DOS effective mass	1.27	for longitudinal direction only, from [SR6]
electron mobility μ_{max}	166 cm^2 V^{-1} s^{-1}	for longitudinal direction only, from [SR6]
hole mobility $\mu_{max,h}$	15.7 cm^2 V^{-1} s^{-1}	for longitudinal direction only, from [SR6]
mobility dependence with temperature	$\mu(T) = \mu_{max} (T/T_0)^{-A}$	assuming $A = 2.5$ (electrons), 2.2 (holes), typical values for monocrystalline Si, $T_0 = 300$ K

TABLE S2. Activated surface trap concentrations used in the finite-element simulations with one fitting parameter, for different nanowire diameters. The temperature is varied from 50 to 400 °C, whereas the NO_2 concentration is fixed at 500 ppm. The trap concentrations N_T are expressed in cm^{-2}, only the active traps are reported; they are recovered from the induced space charge through spatial integral.

Temperature	41 nm	62 nm	78 nm	103 nm	117 nm
50 °C	$2.52 \cdot 10^{11}$	$2.91 \cdot 10^{11}$	$2.49 \cdot 10^{11}$	$1.06 \cdot 10^{11}$	$6.20 \cdot 10^{10}$
100 °C	$3.56 \cdot 10^{11}$	$5.22 \cdot 10^{11}$	$4.11 \cdot 10^{11}$	$4.48 \cdot 10^{11}$	$2.03 \cdot 10^{11}$
150 °C	$4.45 \cdot 10^{11}$	$5.42 \cdot 10^{11}$	$5.45 \cdot 10^{11}$	$5.44 \cdot 10^{11}$	$5.64 \cdot 10^{11}$
200 °C	$5.79 \cdot 10^{11}$	$7.73 \cdot 10^{11}$	$9.41 \cdot 10^{11}$	$1.11 \cdot 10^{12}$	$1.24 \cdot 10^{12}$
250 °C	$6.40 \cdot 10^{11}$	$9.01 \cdot 10^{11}$	$1.05 \cdot 10^{12}$	$1.36 \cdot 10^{12}$	$1.50 \cdot 10^{12}$
300 °C	$6.43 \cdot 10^{11}$	$9.06 \cdot 10^{11}$	$1.05 \cdot 10^{12}$	$1.37 \cdot 10^{12}$	$1.48 \cdot 10^{12}$
350 °C	$6.40 \cdot 10^{11}$	$9.17 \cdot 10^{11}$	$1.09 \cdot 10^{12}$	$1.39 \cdot 10^{12}$	$1.50 \cdot 10^{12}$
400 °C	$6.26 \cdot 10^{11}$	$8.76 \cdot 10^{11}$	$1.03 \cdot 10^{12}$	$1.29 \cdot 10^{12}$	$1.39 \cdot 10^{12}$

TABLE S3. Activated surface trap concentrations used in the finite-element simulations with one fitting parameter, for different nanowire diameters. The NO_2 concentration is varied from 50 to 1000 ppm, whereas the temperature is fixed at 250 °C. The trap concentrations N_T are expressed in cm^{-2}, only the active traps are reported; they are recovered from the induced space charge through spatial integral.

Concentration	41 nm	62 nm	78 nm	103 nm	117 nm
50 ppm	$3.79 \cdot 10^{11}$	$4.44 \cdot 10^{11}$	$4.50 \cdot 10^{11}$	$4.55 \cdot 10^{11}$	$2.57 \cdot 10^{11}$
100 ppm	$5.10 \cdot 10^{11}$	$5.97 \cdot 10^{11}$	$6.17 \cdot 10^{11}$	$8.15 \cdot 10^{12}$	$7.36 \cdot 10^{11}$
200 ppm	$5.60 \cdot 10^{11}$	$7.44 \cdot 10^{11}$	$8.44 \cdot 10^{11}$	$1.05 \cdot 10^{12}$	$1.15 \cdot 10^{12}$
300 ppm	$5.96 \cdot 10^{11}$	$8.52 \cdot 10^{11}$	$9.68 \cdot 10^{11}$	$1.19 \cdot 10^{12}$	$1.33 \cdot 10^{12}$
400 ppm	$6.23 \cdot 10^{11}$	$8.78 \cdot 10^{11}$	$1.02 \cdot 10^{12}$	$1.27 \cdot 10^{12}$	$1.37 \cdot 10^{12}$
500 ppm	$6.40 \cdot 10^{11}$	$9.01 \cdot 10^{11}$	$1.05 \cdot 10^{12}$	$1.36 \cdot 10^{12}$	$1.50 \cdot 10^{12}$
1000 ppm	$6.50 \cdot 10^{11}$	$9.15 \cdot 10^{11}$	$1.12 \cdot 10^{12}$	$1.43 \cdot 10^{12}$	$1.56 \cdot 10^{12}$

TABLE S4. Adsorption and desorption time constants, expressed in s, calculated according to the two proposed methods, i.e. linear interpolation (subscript "li") and estimation from the transient duration (subscript "td"). The NO$_2$ concentration is fixed at 500 ppm, whereas the temperature is varied in the range 200÷400 °C. The nanowire diameter is D = 78 nm.

Temperature	Time constants (s)			
	$\tau_{ads,li}$	$\tau_{des,li}$	$\tau_{ads,td}$	$\tau_{des,td}$
200 °C	2.54	3.11	1.69	2.41
250 °C	1.96	2.14	1.14	2.10
300 °C	1.33	1.87	1.33	1.95
350 °C	0.91	1.05	1.12	1.85
400 °C	0.61	1.32	1.33	1.68

TABLE S5. Surface trap concentrations, expressed in cm^{-2}, calculated according to the two proposed methods, i.e. linear interpolation (subscript "li") and estimation from the transient duration (subscript "td"). The NO$_2$ concentration is fixed at 500 ppm, whereas the temperature is varied in the range 200÷400 °C. The considered nanowire diameter is D = 78 nm. Only the active traps are reported; they are recovered from the induced space charge through spatial integral.

Temperature	Surface trap concentrations	
	$N_{T,li}$	$N_{T,td}$
200 °C	$1.156 \cdot 10^{12}$	$1.134 \cdot 10^{12}$
250 °C	$1.165 \cdot 10^{12}$	$1.154 \cdot 10^{12}$
300 °C	$1.157 \cdot 10^{12}$	$1.137 \cdot 10^{12}$
350 °C	$1.159 \cdot 10^{12}$	$1.15 \cdot 10^{12}$
400 °C	$1.14 \cdot 10^{12}$	$1.12 \cdot 10^{12}$

Supplementary references

[SR1] W. Matysiak, T. Tanski, W. Smok, 2020. Study of optical and dielectric constants of hybrid SnO_2 electrospun nanostructures. *Applied Physics A* **126** 115.

[SR2] N. Oka, S. Yamada, T. Yagi, N. Taketoshi, J. Jia, Y. Shigesato, 2014. Thermophysical properties of SnO2-based transparent conductive films: Effect of dopant species and structure compared with In_2O_3-, ZnO-, and TiO_2-based films. *Journal of Materials Research* **29** 1579-1584.

[SR3] P. Turkes, C. Plunkte, R. Helbig, 1980. Thermal conductivity of SnO_2 single crystals. *Journal of Physics C: Solid State Physics* **13** 4941-4951.

[SR4] S. Luo, J. Fan, W. Liu, M. Zhang, Z. Song, C. Lin, X. Wu, P.K. Chu, 2006. Synthesis and low-temperature photoluminescence properties of SnO_2 nanowires and nanobelts. *Nanotechnology* **17** 1695-1699.

[SR5] V. Stevanovic, S. Lany, D.S. Ginley, W. Tumas, A. Zunger, 2014. Assessing capability of semiconductors to split water using ionization potentials and electron affinities only. *Physical Chemistry Chemical Physics* **16** 3706-3714.

[SR6] Y. Hu, J. Hwang, Y. Lee, P. Conlin, D.G. Schlom, S. Datta, K. Cho, 2019. First principles calculations of intrinsic mobilities in tin-based oxide semiconductors SnO, SnO_2, and Ta_2SnO_6. *Journal of Applied Physics* **126** 185701.

Dr. Roberto Guarino is a Post-doctoral Fellow at the Swiss Plasma Center of EPFL (Villigen PSI, Switzerland), where he works on the multi-physical and multi-scale design of superconducting magnets for fusion reactors. He received his B.Sc. in Materials Engineering and his M.Sc. in Mechanical Engineering from the Politecnico di Torino (Torino, Italy). He earned a Ph.D. in Civil, Environmental and Mechanical Engineering from the University of Trento (Trento, Italy) with a thesis on the modelling and simulation of tribology of complex interfaces. His research is focused, on one side, on fundamental aspects in solid and structural mechanics, as well as on fracture mechanics. On the other side, he is working on applied research activities in superconductivity and electronics, including sensors and energy. He co-authored more than 20 publications on international peer-reviewed journals and he is co-inventor of several patent applications.

Mr. Fabrizio Mo received the M.Sc. degree with honours (*Magna cum Laude*) in Electronic Engineering from the Politecnico di Torino (Torino, Italy) in 2020, with a thesis on molecular gas sensors for single-molecule detection of toxicants. He is currently pursuing a Ph.D. in Electrical, Electronics and Communication Engineering at Politecnico di Torino. His primary research interests are molecular sensors, semiconductor sensors and relative front-end electronics.

Dr. Yuri Ardesi received the B.Sc. in 2015 and the M.Sc. degrees in Electronics Engineering for Micro and Nanosystems in 2017 from the Politecnico di Torino (Torino, Italy), where he continued as a Ph.D. student in Electrical, Electronics and Communication Engineering. His primary research interests are molecular technologies for sensing and beyond-CMOS computing, with a particular focus on molecular Field-Coupled Nanocomputing. Currently, he is a Research Associate at the Department of Electronics and Telecommunications of Politecnico di Torino.

Dr. Andrea Gaiardo obtained the M.Sc. degree in Chemistry (*Magna cum Laude*) from the University of Ferrara, (Ferrara, Italy) in 2013. He received the Ph.D. degree in Physics from the University of Ferrara in 2018. His work is focused on the research and development of gas sensing systems for several applications, including precision agriculture and outdoor air quality monitoring. In this field, he has published more than 30 articles (H-Index = 13, source Scopus, 04/2022), and he has been guest editor of

three special issues. He has collaborated in both national and European projects. Currently, he is a researcher in the Micro-Nano Facilities group of the Bruno Kessler Foundation.

Dr. Matteo Tonezzer graduated with honours in Physics and received his Ph.D. degree from the Faculty of Physics of the University of Trento (Trento, Italy) in 2011. His thesis was about the optimisation of inorganic and organic nanostructured materials toward gas sensing. In 2011, he won the Young Scientist Award from the European Materials Research Society (EMRS). He worked in research centers in France (ESRF), Brazil (UFMG), Vietnam (HUST), USA (GaTech) and South Korea (INHA). He is currently working for IMEM at the Italian National Research Council, where his major research interest is the synthesis and characterization of nanostructured materials.

Mr. Sergio Guarino is pursuing a B.Sc. in Information and Communication Technologies at HEPIA (Geneva, Switzerland), where he is specialising in network infrastructure and cybersecurity. After technical studies in Electrical Engineering and Automation, he was selected as an Electronics and Robotics technician at the European Organization for Nuclear Research (CERN) (Geneva, Switzerland), where he worked on control electronics and robotic systems for the Large Hadron Collider. He is also co-founder and Member of the Board of Koral Technologies Srl (Trento, Italy), where he is co-inventor of several patent applications.

Prof. Gianluca Piccinini received the Dr. Ing. and Ph.D. degrees in Electronics Engineering in 1986 and 1990, respectively. He has been a Full Professor since 2006 at the Department of Electronics of the Politecnico di Torino (Torino, Italy), where he teaches electron devices and integrated system technology. His research activities were initially focused on VLSI architectures for artificial intelligence and moved, during the 1990s, toward the physical design of VLSI systems for high-rate and high-speed transmission and coding algorithms. His current research interests include the introduction of new technologies as molecular electronics in integrated systems, where he studies transport, advanced microfabrication, and self-assembly technologies in molecular-scale systems. He is the author and co-author of more than 120 published works and is the holder of one international patent.